lubricants

MDPI

Article

Tribology and Hot Corrosion Behavior of MCrAlY-Based Multicomponent Coatings Containing Copper

Bruno C. N. M. de Castilho [1], Navid Sharifi [2], Mary Makowiec [3], Pantcho Stoyanov [4], Christian Moreau [2] and Richard R. Chromik [1,*]

[1] Department of Mining and Materials Engineering, McGill University, M.H. Wong Building, 3610 University Street, Montreal, QC H3A 0C5, Canada; bruno.noronhamarquesdecastilho@mail.mcgill.ca
[2] Department of Mechanical, Industrial and Aerospace Engineering, Concordia University, EV Building, 1515 St. Catherine W., Montreal, QC H3G 2W1, Canada; navid.sharifi@concordia.ca (N.S.); christian.moreau@concordia.ca (C.M.)
[3] Pratt & Whitney, 400 Main Street, East Hartford, CT 06118, USA; mary.makowiec@prattwhitney.com
[4] Department of Chemical and Materials Engineering, Concordia University, EV Building, 1515 St. Catherine W., Montreal, QC H3G 2W1, Canada; pantcho.stoyanov@concordia.ca
* Correspondence: richard.chromik@mcgill.ca

Abstract: The use of composite coatings containing solid lubricants is widely reported in the literature, in particular thermally sprayed coatings containing silver. However, these coatings are often limited in their maximum operating temperature due to the melting point of silver and due to reactions between the components at temperatures above 500 °C. In this study, a novel coating is proposed, which consists of an MCrAlY-based matrix and the addition of components (Cu, Mo, and BaF_2) to improve the wear resistance at elevated temperatures. The coatings were sprayed by high-velocity oxy-fuel, heat-treated at 1040 °C, and tribologically tested at room and elevated temperatures. Raman spectroscopy and scanning electron microscopy were used on worn and unworn regions of the coating to characterize the changes in microstructure caused by wear. The coatings were also exposed to oxidation and hot corrosion conditions to evaluate the resistance to high-temperature environments. The results have shown an improvement in wear rates of the coatings upon heat treatment and the formation of a smooth tribolayer at 300 °C. The as-sprayed coating was able to withstand the attack by molten salts without exposing the substrate, and minor weight gain was observed, indicating that the MCrAlY matrix was effective to protect the coating and the substrate against damages induced by salt penetration.

Keywords: solid lubrication; MCrAlYX; hot corrosion; oxidation; sliding wear

Received: 21 December 2024
Revised: 26 January 2025
Accepted: 5 February 2025
Published: 7 February 2025

Citation: de Castilho, B.C.N.M.; Sharifi, N.; Makowiec, M.; Stoyanov, P.; Moreau, C.; Chromik, R.R. Tribology and Hot Corrosion Behavior of MCrAlY-Based Multicomponent Coatings Containing Copper. *Lubricants* **2025**, *13*, 73. https://doi.org/10.3390/lubricants13020073

1. Introduction

Coatings that use multiple components to provide solid lubrication at high temperatures have been widely reported in the literature. Some of the main representatives of these materials are the coatings proposed by Sliney [1] and further developed by Della-Corte [2], also known as the PS series (from PS100 to PS400). These coatings contain a nickel-based matrix (NiCr, NiMoAl, and others), a hardening phase (chromium oxide or chromium carbide), and solid lubricants for the medium and high-temperature conditions (silver and barium/calcium eutectic, respectively). Such coatings have shown good wear performance and low friction coefficients at high-temperature conditions, particularly for thrust-washer [3,4], airfoil bearing [5], and steam turbine [6] applications.

Nevertheless, there are some limitations when these coatings must perform at temperatures above 600 °C. The PS300 (Cr_2O_3-NiCr-Ag-BaF_2/CaF_2), for instance, with 60 wt.%

of Cr_2O_3, suffered from delamination issues caused by the mismatch of the coefficient of thermal expansion (CTE) between the coating and the X750 substrate [2]. Such an issue was solved with the development of the PS304 (NiCr-Cr_2O_3-Ag-BaF_2/CaF_2), by increasing the amount of NiCr to 60 wt.% and reducing the amount of Cr_2O_3 to 20 wt.%, thus achieving a similar CTE between coating and substrate [2]. However, the NiCr had an abnormal expansion of the coating at elevated temperatures [7] due to the formation of chromium fluorides inside the NiCr matrix [8].

Built upon the PS304 composition, the PS400 (NiMoAl-Cr_2O_3-Ag-BaF_2/CaF_2) showed an improved performance at higher temperatures compared to the PS304, with wear rates of 6–8 $\times$ 10^{-6} $mm^3/N{\cdot}m$ and no significant expansion at high temperature [8,9]. However, when the PS400 coatings were tested at 927 °C, studies have shown that the coating starts failing due to the proximity to the silver melting point, causing instability and severe wear by scuffing [10]. Furthermore, under oxidation and hot corrosion conditions, these coatings also failed to protect the substrate, forming oxides and sulfides at the coating–substrate interface, and some of the coatings spalling after being exposed to 950 °C [11].

Several attempts were made to further improve the performance of these coatings by changing either the spray method or the composition. Kim et al. changed the spraying method from APS to HVOF, but limited success was observed in deposition efficiency with the commercially available feedstock [12]. Some studies focused on changing the metallic matrix by using TiAl [13], NiAl [14], NiCrAlY [15], and NiCoCrAlTaY [16] while keeping silver as a solid lubricant. When testing these coatings at high-temperature conditions, it is often observed that the formation of ternary oxides, often silver-based ones, provides lubrication at high temperatures [15–17].

As a soft metal solid lubricant, silver is a good compromise between performance, cost, and toxicity. While gold and platinum are good candidates due to their chemical inertia, the high cost involved in manufacturing such powder is prohibitive depending on the application. Lead is also a possible candidate, but it faces severe restrictions due to the toxicity to humans, animals, and the environment [18].

One material, however, that often does not appear as a part of multicomponent coatings is copper. The immediate oxidation of copper at high temperature often means that such material is not considered a solid lubricant, while causing detrimental effects on the coating's tribological properties. However, some authors claim some limited wear-resistant and lubricating properties of copper. Yuan et al. have shown that an addition of up to 30 wt.% of copper in a matrix of WC-Co and using BaF_2-CaF_2 can decrease the wear rate from 25.7 $\pm$ 2.8 $\times$ 10^{-5} $mm^3/N{\cdot}m$ to 1.30 $\pm$ 0.03 $\times$ 10^{-5} $mm^3/N{\cdot}m$ and the friction from 0.38 to 0.02 when testing at room temperature [19]. Another study has shown that copper-based ternary oxides have the potential of outperforming silver-based ternaries at a high testing temperature [20]. There is, however, a lack of studies using copper as one of the elements on multicomponent coatings for tribological applications [18].

In an attempt to extend the operating temperature of multicomponent coatings and improve their oxidation and hot corrosion resistance, a new composition is proposed containing copper, barium fluoride, molybdenum and a matrix of NiCoCrAlYTa. The coating was deposited by high-velocity oxyfuel (HVOF), characterized, and tribologically tested at room and elevated temperatures. Furthermore, oxidation and hot corrosion tests were performed to verify if changing the matrix material to MCrAlY would improve the hot corrosion behavior of these coatings.

2. Materials and Methods

Coatings were produced using a mixture of powders containing 80 wt.% NiCoCrAlYTa (Oerlikon, Pfäffikon, Switzerland), 10 wt.% Cu (Oerlikon, Switzerland), 5 wt.% Mo (Eutectic,

Vaudreuil-Dorion, QC, Canada) and 5 wt.% BaF_2 (Eutectic, Canada). The powder size distribution was measured for each individual composition and for the mixture, using a laser diffraction FlowSync powder size analyzer (Microtrac MRB, York, PA, USA). Then, the mixed powder was prepared by weighing each individual component and mixing it in a VH-2 powder mixer (MXBAOHENG, Zhejiang, China) for 1 h and then sprayed by HVOF with a Diamondjet 2700 gun (Oerlikon, Pfäffikon, Switzerland). The coatings for tribological testing were deposited on stainless steel substrates using the spray conditions provided by the manufacturer of the matrix component, shown in Table 1. For hot corrosion tests, the coatings were deposited on an X750 substrate (150 mm × 150 mm × 7 mm) using the same spray conditions.

Table 1. HVOF deposition parameters.

Parameter	Value
Feed rate (g/min)	38
Oxygen flow rate (nlpm)	152
Propylene (fuel) (nlpm)	85
Air (nlpm)	284
Transverse speed (mm/s)	1000
Spraying distance (mm)	250
Number of passes	35

After the deposition, the coated surface of all samples was ground and polished following standard polishing procedures up to a mirror finish using colloidal silica (0.05 μm) before tribological testing. Some polished samples were heat treated at 1040 °C for four hours to induce the formation of oxides at the top surface before being tribologically tested.

Wear tests were performed against alumina counterfaces (6.35 mm diameter) at room temperature and elevated temperature (300 °C) using a TRB tribometer (Anton-Paar, Graz, Austria) equipped with a high-temperature module. A load of 5 N was used, with a reciprocating frequency of 1 Hz in a 10 mm track to a total of 5000 cycles (100 m). The friction coefficient was recorded throughout the whole test, and the average of each cycle was taken at the middle of the wear track (from 2 mm to 8 mm).

The wear tracks were analyzed by a NewView light profilometer (Zygo Corporation, Middlefield, CT, USA). For non-heat-treated samples, the whole track was scanned, and 30 profiles perpendicular to the sliding direction were taken across the track. To determine the wear rate (K), the worn area (A_w) was calculated for each profile and averaged, and the result was multiplied by the total track length (L) and divided by the applied load (W) and total distance (d), following Equation (1):

$$K_{sample} = \frac{A_w * L}{W * d} \quad (1)$$

For heat-treated samples, the wear depths were comparable to the surface roughness, and because of that, only the surface roughness inside and outside the wear track was reported here.

For the counterfaces, the same light profilometer was used, but instead of measuring profiles, the worn volume (V_w) was directly measured, and then the following Equation (2) was used to calculate the wear rate:

$$K_{counterface} = \frac{V_w}{W * d} \quad (2)$$

Scanning electron microscopy (SEM) was used to characterize the powder feedstock, the coating, and the worn tracks. The SEM (SU3500, Hitachi, Tokyo, Japan) was equipped

with secondary electron (SE) and backscattered electron (BSE) detectors as well as an ultra-variable pressure detector (UVD), which operated in low vacuum conditions to minimize charging effects. Furthermore, electron dispersive spectroscopy (EDS) was used to identify the elements present in the different regions of the powder and of the coating. Coating thickness was measured at the cross-section of the coating using BSE images, with 10 measurements taken in each image in three different locations of each cross-section.

A D8 Discovery diffractometer (Bruker, Billerica, MA, USA) was used with a Co-source (λ = 1.78897 Å) and 2θ ranging from 20° to 120° to identify the phases on as-sprayed and heat-treated coatings. A voltage of 35 kV and a current of 45 mA were used, and the phases were indexed using ICDD JCPDS references.

The mechanical properties of the coatings were assessed by microhardness and nanoindentation. For the microhardness tests, 15 indents were made on the cross-section of the as-sprayed and heat-treated coatings with a load of 25 gf using a Vickers indenter (Clark Microhardness Tester, Lenexa, KS, USA).

For the nanoindentation tests, a Triboindenter (Hysitron Inc., Eden Prairie, MN, USA) was used with a Berkovich tip. The tests were performed on the cross-section of the coatings, and a hundred indents in a matrix of 10 × 10 indents spaced by 10 μm were made for each coating using a load of 5 mN and a load–hold–unload time of 5 s–2 s–5 s. The hardness and elastic modulus were calculated by the Oliver and Pharr method [21] and considering the Poisson ratio of 0.3. Then, after the test, BSE contrast and EDS analysis were used to determine in which component each indent fell. For this study, only indents that were on the matrix were reported.

Raman spectra were collected with a Raman spectrometer (inVia, Renishaw, UK) using an Ar+ based laser (λ = 514.5 nm) in different locations of the wear tracks and the unworn heat-treated surface to characterize the compounds being formed after heat treatment and during the wear test at room and high temperatures for all samples.

For the oxidation and hot corrosion tests, 1 cm^2 square samples were cut by water jet from the as-sprayed X750 plate, and the coated surfaces were ground and polished up to 3 μm diamond solution. For the oxidation test, the samples were first weighed to determine the weight before the test (w_0), and then inserted in a FB1315M (Fisher Scientific, Waltham, MA, USA) for 24 h at the test temperature (either 550 °C, 850 °C, or 950 °C). Then, the samples were cooled down to room temperature in open air and weighed again to determine the final weight (w_f). The weight gain/loss by surface area was calculated by subtracting w_0 from w_f and dividing by the surface area, which was measured with a digital caliper (Mastercraft, Newburgh, NY, USA).

For the hot corrosion test, a solution containing 0.4 g of salt (60 wt.% Na_2SO_4 and 40 wt.% $MgSO_4$) in 10 mL of deionized water was prepared. A total of 50 μL of this solution was poured with a micropipette on top of each sample after determining the initial weight of the sample without salt (w_0). After the salt solution was applied, the sample was dried inside the furnace at 100 °C for 15–20 min. Then, the samples were weighed to determine the initial weight with salt (w_{0s}) and added back to the furnace, which was set to the target testing temperature (either 550 °C, 850 °C, or 950 °C). After 24 h, the samples were removed from the furnace, cooled down in open air, and weighed to determine the final weight with salt (w_{fs}). The total weight gain/loss per unit area was calculated by subtracting w_{0s} from w_{fs} and dividing by the coated area. For both hot corrosion and oxidation, three repeats were performed for each temperature.

3. Results and Discussion

3.1. Powder Characterization

Figure 1 shows the powder size distribution of each constituent of the powder mixture (dashed lines) and of the powder after mixing, as well as the secondary electron (SE) images of each powder component. Copper had the highest D50 of 50.6 µm and the narrowest distribution, while the D50 of NiCoCrAlYTa was 29.1 µm. A similar D50 was observed for molybdenum (24.4 µm), and the smallest D50 was found for the BaF_2 (15.4 µm).

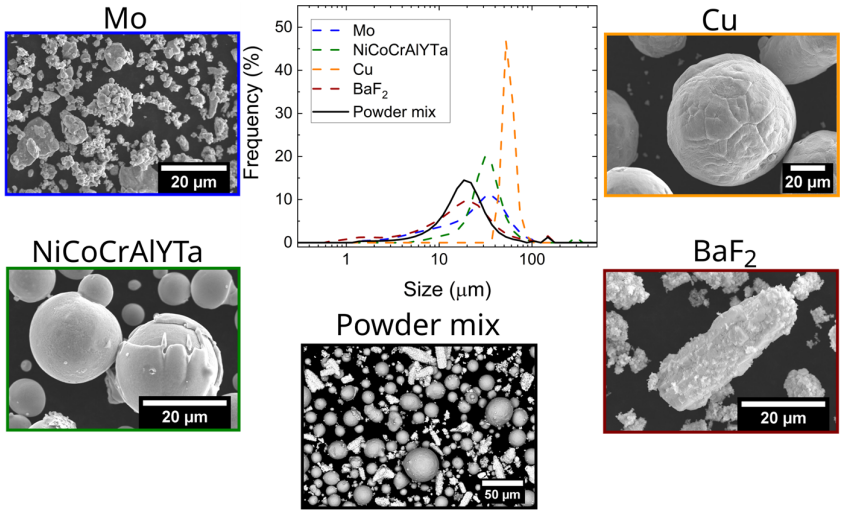

Figure 1. Images showing each individual powder morphology with secondary electron (SE) images, a backscattered electron (BSE) image of the powder after mixing, and the powder size distribution of all the powder feedstock.

After mixing, the D50 of the powder mixture was 16.9 µm, which is inside the range for HVOF spraying. Meanwhile, the backscattered image of the mixed feedstock is shown at the bottom of Figure 1. The powder morphology of the different components was widely different, with Cu and MCrAlY powders presenting spherical morphology while BaF_2 and Mo presented irregular-shaped morphologies.

3.2. Coating Characterization

Figure 2A shows the cross-section of the as-sprayed coating, with a thickness of 594 ± 8 µm, and in Figure 2B an EDS map of the as-sprayed coating is shown, confirming the successful spray of all the different components of the powder mixture. Oxidation is observed at some locations of the cross-section, matching the regions rich in aluminum, indicating the formation of aluminum oxides during the spray. However, aluminum is still observed inside the MCrAlY splats, indicating that only part of the aluminum was oxidized during the spray. EDS analysis on such a region showed less than 3 wt.% of oxygen, concentrated mainly in regions of the MCrAlY splat boundaries. No oxidation was observed either for the BaF_2, Mo, or Cu components.

In Figure 3A, the cross-section of the heat-treated coating is observed, with a thickness of 477 ± 9 µm. The reduction in thickness observed here is caused by the grinding and polishing of the top surface before the heat treatment. Porosity is observed throughout the whole image of the heat-treated coating, while a layer of oxides is observed at the top surface.

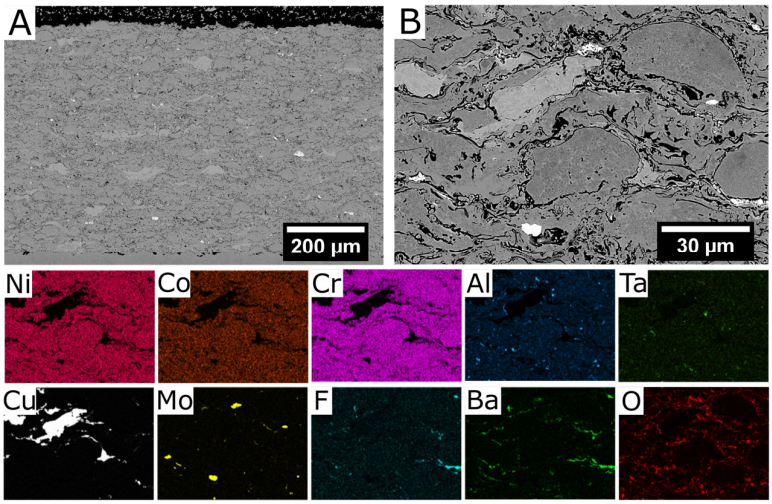

Figure 2. Cross-section observation with BSE signal and EDS maps of the as-sprayed coating: (**A**) lower magnification and (**B**) higher magnification images.

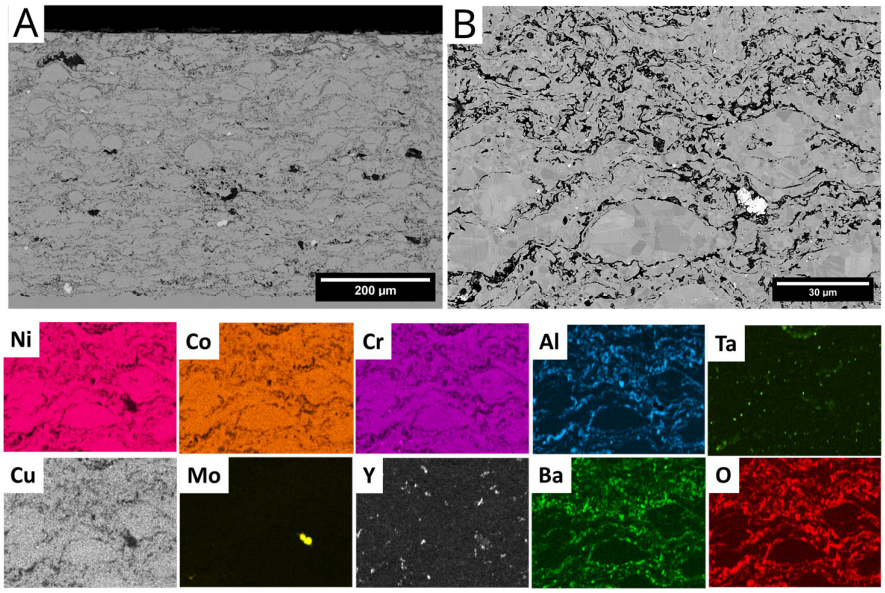

Figure 3. Cross-section observation with BSE signal and EDS maps of the heat-treated coating: (**A**) lower magnification and (**B**) higher magnification images.

After heat-treating, however, the elemental distribution changed significantly, as shown in the EDS mapping of Figure 3B. The copper splats, once observed throughout the coating (Figure 2A,B), are no longer observed after heat treatment (Figure 3A,B), and the porosity observed in such coatings matches the shape and possible positions of the copper splats. Furthermore, copper is observed throughout the whole detailed region (Figure 3B), matching the location in which nickel, cobalt, and chromium are present. Such a feature indicates that copper diffused through the MCrAlY matrix, leaving pores inside the heat-treated coating. Oxygen content increased in the analyzed region, reaching up to 5.8 wt.%, indicating that oxygen started to permeate through the coating. Nevertheless, the coating/substrate interface did not show any signs of oxidation, indicating that the coating protected the substrate against oxidation.

Different from the as-sprayed coating, fluorine is no longer observed in the selected region, and the barium-rich regions match the oxidized regions in the EDS, indicating the oxidation of the BaF_2 and possible release of fluorine during the heat treatment. The regions rich in barium are now also rich in aluminum, which could indicate the formation

of a ternary oxide between these elements or a mixed oxide region. Tantalum is present in the form of bright precipitates, both inside the matrix splats and around it. EDS point analysis showed that, in such locations, tantalum, nickel, cobalt, and chromium are the predominant elements, with no presence of oxygen.

Near the surface, shown in Figure 4, oxidation occurs in a more intense manner, and layers of oxides are observed. In close contact with the unoxidized splats, a layer of aluminum oxide is observed, being formed by the oxidation of the MCrAlY component. However, a complex microstructure can be observed on top of this aluminum layer, composed of many of the elements of the coating. In these regions, it is reasonable to assume that the formation of mixed oxides happened, which could potentially have locally melted the materials in these regions, mainly driven by the interdiffusion between the multiple elements. In such regions, precipitates of tantalum can be observed, as well as a mixture of nickel, cobalt, chromium, barium, and molybdenum. Furthermore, there are overlaps between the regions rich in barium and molybdenum and barium and chromium, suggesting the formation of ternary oxides between these elements.

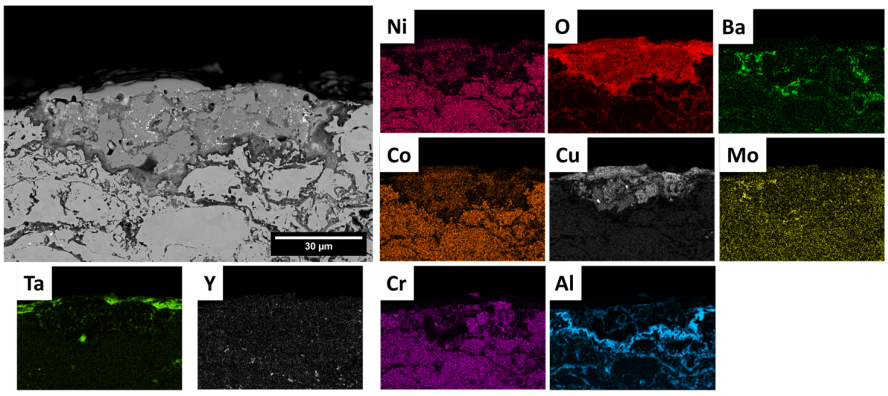

Figure 4. Cross-section observation near the surface with BSE signal and EDS maps of the heat-treated coating.

SEM images were also taken on the top of the coating after heat treatment, in Figure 5. The top surface was full of different oxides, formed by the interdiffusion of elements among the different components, and in agreement with the components observed in Figure 4. In a general manner, four different regions can be observed in Figure 5. A considerable portion of the surface is covered by a dark-contrast phase, which is rich in aluminum and oxygen (among other elements). Then, the bright regions are rich in barium, molybdenum, chromium, and oxygen. The light gray region (bottom right) shows non-oxidized regions, and they are composed of regions in which MCrAlY was not oxidized and/or regions where the aluminum oxide cover was spalled. However, these regions also show the presence of copper, another piece of evidence of copper diffusion towards the MCrAlY matrix. Lastly, the region shown on the top of the image and presented in more detail in Figure 5B shows the formation of dendrites rich in copper and oxygen immersed in a (Ni, Co, and Cr) oxide region. It is hypothesized that in these regions, localized melting happened due to the interdiffusion of copper into the MCrAlY matrix, forming pools of molten material, which then solidified as copper oxide dendrites and a segregating phase that is composed of a solution of MCrAlY elements (but mainly nickel) and oxygen.

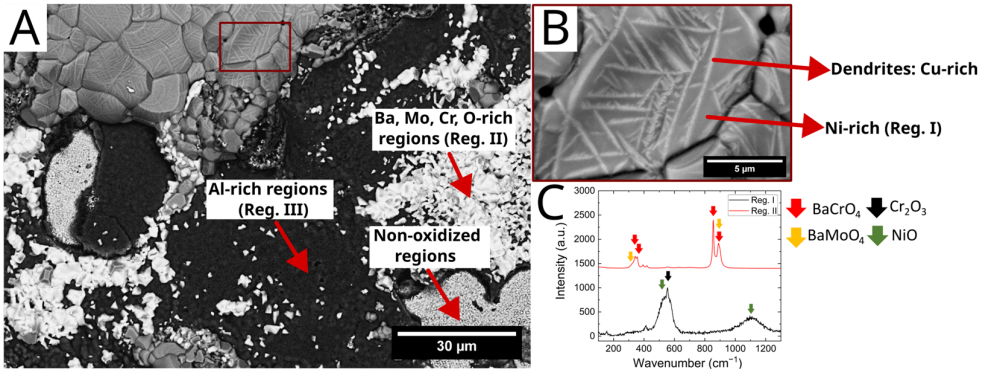

Figure 5. (**A**) New phases formed at the top surface; (**B**) in detail a region showing a dendritic structure formed at the surface and rich in copper and oxygen, indicating the localized melting of the copper oxide inside a (Ni, Co, and Cu) oxide-rich region; and (**C**) Raman spectra collected in various locations of the surface.

Raman spectra were taken on several locations of the surface of the heat-treated coating, and they are shown in Figure 5C. The presence of $BaCrO_4$ (peaks at 350 cm^{-1}, 854 cm^{-1} and 894 cm^{-1}), $BaMoO_4$ (convoluted peaks at 322 cm^{-1} and 899 cm^{-1}), NiO (at 535 cm^{-1} and 1100 cm^{-1}), and Cr_2O_3 (convoluted at 553 cm^{-1}) can be confirmed in different locations of the surface, formed during the heat treatment of the coating.

X-ray diffraction was also used to characterize the phases produced after spraying and after the heat treatment on unworn coatings, as shown in Figure 6. On the as-sprayed coating, nickel peaks were observed but shifted, indicating the solid solution of the other components of the NiCoCrAlYTa component with Ni_3Al also present which is commonly observed in MCrAlY-based powder and coatings [22–24]. The deposition of the other components of the coating (BaF_2, Cu, and Mo) was also confirmed by XRD.

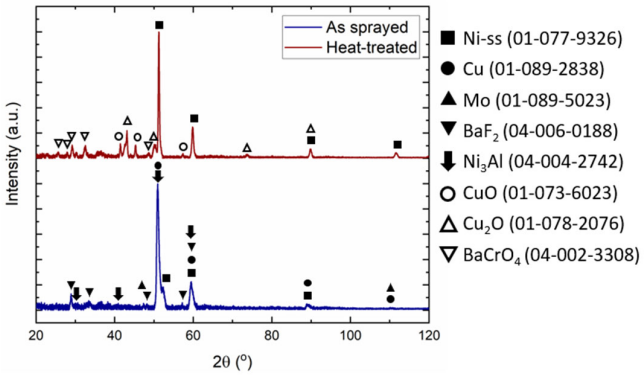

Figure 6. XRD of the coating in as-sprayed condition and after heat treatment.

Upon heat treatment, the interdiffusion of the elements of the different components combined with the oxidation of some of them produced new phases in the coating. Two different copper oxide phases were observed (CuO and Cu_2O), as well as the formation of ternary oxides between barium and chromium ($BaCrO_4$). The nickel peaks are still shifted, but now towards higher values of 2θ, while the peaks of Ni_3Al no longer appear. Based on the information from the EDS map and the XRD data, copper diffuses inside the original MCrAlY splats, while Al diffuses outwards, thus depleting the Ni_3Al component, which not only causes the disappearance of the Ni_3Al peaks but also the shift in the nickel peaks.

A comparison of the microhardness at the cross-section of the as-sprayed and heat-treated coating was also performed. The heat-treated sample had a microhardness value of 495 ± 57 HV, while the as-sprayed one showed a microhardness value of 397 ± 107 HV. Such high deviation on the as-sprayed sample is an indication of the non-homogeneity of

the coating, and the higher hardness observed on the heat-treated coating is a combined effect of the incorporation of copper into the MCrAlY matrix and the oxidation of the aluminum around the splats, which increased the overall hardness of the coating.

To assess how the incorporation of copper contributes to the modification of the mechanical properties of the matrix, nanoindentation was used on the cross-section of both coatings. The results show that, for the matrix component on the as-sprayed coating, a hardness of 5.4 ± 0.6 GPa and an elastic modulus of 176 ± 18 GPa were measured. For the matrix component after heat treatment; however, a hardness of 5.5 ± 0.3 GPa and an elastic modulus of 234 ± 15 GPa were measured. Such an increase in elastic modulus could be justified by the incorporation of copper in the matrix happening simultaneously with the depletion of aluminum, since copper has a higher elastic modulus than aluminum ($E_{Cu,\ bulk}$ = 110 GPa, $E_{Al,\ bulk}$ = 69 GPa).

3.3. Friction and Wear Performance

Friction curves are shown in Figure 7A (room temperature testing) and Figure 7B (300 °C testing). For the as-sprayed sample, at room temperature, an unstable friction coefficient is observed, which never reaches a plateau. Friction values oscillate, especially after 1000–1500 cycles, and many peaks at approximately 0.7 are observed. Meanwhile, the heat-treated sample showed a peak of 0.85 in the initial stages of testing, after 40–50 cycles, followed by a sharp decrease, then another peak at approximately 0.75, followed by a steady decrease and stabilization after 3000 cycles.

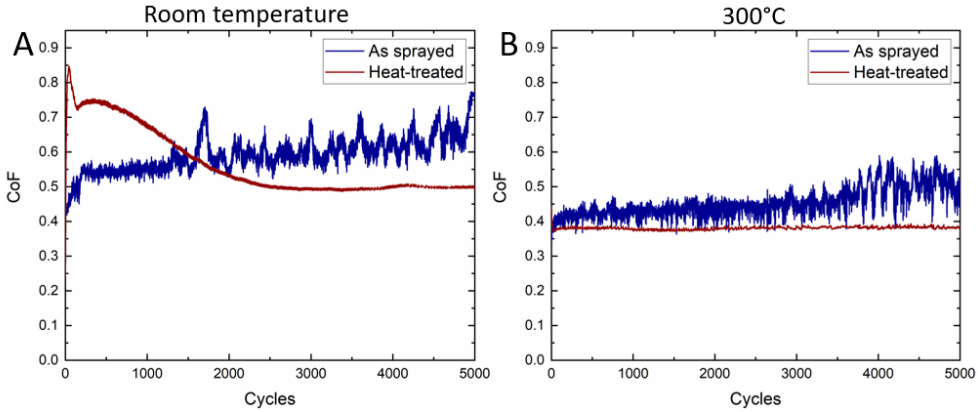

Figure 7. Comparison between friction curves of as-sprayed and heat-treated coatings tested at (**A**) room temperature and (**B**) 300 °C.

At the elevated temperature testing condition, the friction curves for the as-sprayed sample show fewer fluctuations, but again, no plateau in friction is observed for these samples. Meanwhile, for the heat-treated sample, the friction immediately drops after the initial 10 cycles and remains steady at approximately 0.38 throughout the whole test.

To compare the multiple test conditions, the averages of the friction coefficient at room temperature and high temperature are shown in Figure 8A, with only the last 2000 cycles of each test being taken after the three repetitions. The as-sprayed samples showed not only higher friction but also higher standard deviation, a consequence of the unstable behavior during testing.

Wear rates for the as-sprayed coatings were calculated and are shown in Figure 8B, with a higher wear rate for the sample tested at elevated temperature. For the heat-treated samples, because of the rougher surface after heat treating, an accurate measurement of the wear rate was not possible to be acquired since the track depth was approximately in the same order of magnitude as the roughness. Instead, a comparison between the profiles extracted from the tracks of the as-sprayed and heat-treated samples is shown in Figure 8C.

The main difference in the track profile between the tests at room temperature and elevated temperature on the heat-treated sample is the width of the track, which is wider for the test at room temperature.

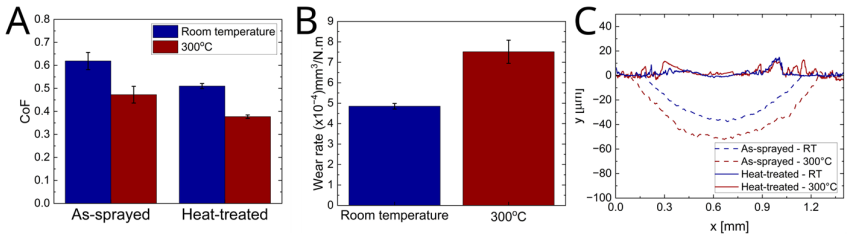

Figure 8. (**A**) Average friction coefficient on the last 2000 cycles for all samples and test conditions after three repeats; (**B**) wear rate for the as-sprayed samples tested at room temperature and 300 °C; and (**C**) comparison between cross-section profiles of the wear track extracted from as-sprayed and heat-treated samples.

Measurements of roughness inside and outside the wear track were taken using the light profilometer and show a polishing effect of the alumina against the surface of the samples. Unworn regions of the heat-treated samples show an R_a of 1.8 ± 0.4 µm in an area of 0.17 mm × 0.17 mm, while for the worn region of the same samples tested at room temperature, the R_a was 0.42 ± 0.02 µm, and at high-temperature testing, the R_a was 0.46 ± 0.07 µm.

3.4. Wear Track Characterization

Figure 9 shows BSE images of the wear track after testing the as-sprayed samples at room temperature (Figure 9A,B) and at 300 °C (Figure 9C,D). In Figure 9E, the Raman spectra of the wear tracks tested at room and elevated temperatures are shown, as well as the spectrum for an unworn region after elevated temperature testing. EDS analysis (Table A1, Appendix A) was used to identify the chemical composition of the different contrasts in the BSE images. At room temperature (Figure 9A,B), the light gray regions (marked with number 1) show low concentrations of oxygen (below 2 wt.%) and copper (below 3 wt.%) and no fluorine or molybdenum, indicating locations in which pristine MCrAlY is present. The bright contrast, marked in blue, shows regions with Mo and BaF_2 (which have similar contrast in the image). The dark contrast regions (marked with number 2), however, are rich in oxygen (26 ± 2 wt.%) and copper (from 15 ± 3 wt%), with signs of adhesive wear and plastic deformation indicated by the red arrows. In those regions, a mix of the elements of the matrix, combined with copper and oxygen, indicates the formation of an oxidized mechanically mixed layer.

On the samples tested at 300 °C (Figure 9C,D), oxidized patches are also observed, but at this testing temperature the patches are smoother than observed at room temperature, which could indicate the compaction of the oxides at the contact interface. Another feature is the presence of debris islands attached to the tribolayer, which are not observed in the room temperature testing condition. These small debris particles could potentially be the precursors of the patches observed throughout the track upon further mixing with the other components and further oxidation. In Figure 9C,D, the bright contrast still represents regions with BaF_2 and/or Mo, but the light gray region, which before represented regions with MCrAlY with low oxidation, now shows minor oxidation (point 4 up to 5 wt.%). The dark patches (point 3) show similar chemical composition at room and high temperature, an oxidized mix of elements from MCrAlY and copper. Some regions, however, show high concentrations of copper and oxygen (indicated by the number 5 in Figure 10D), in which copper content reaches more than 50 wt.%. Copper- and oxygen-rich regions are

also observed outside the wear track, indicating the immediate oxidation of the copper component when exposed to atmospheric conditions during the high-temperature test.

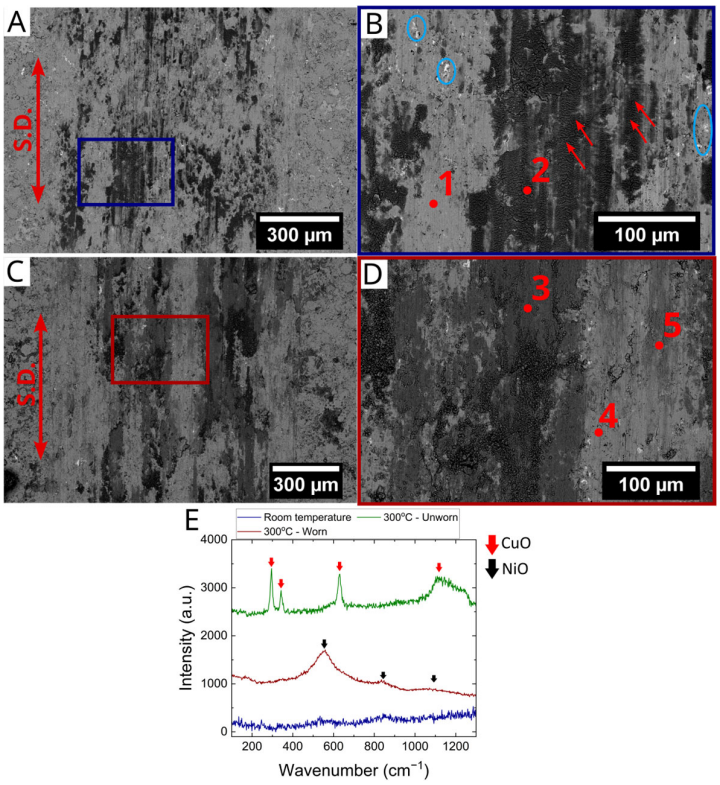

Figure 9. BSE images of the wear track of the samples tested at (**A**) room temperature and (**C**) 300 °C; (**B**,**D**) are higher magnification images of (**A**,**C**), respectively. In (**B**), the blue marks indicate the presence of Mo and BaF_2 and the arrows indicate the regions with evidence of adhesive wear and (**E**) shows Raman spectra taken at the top surface.

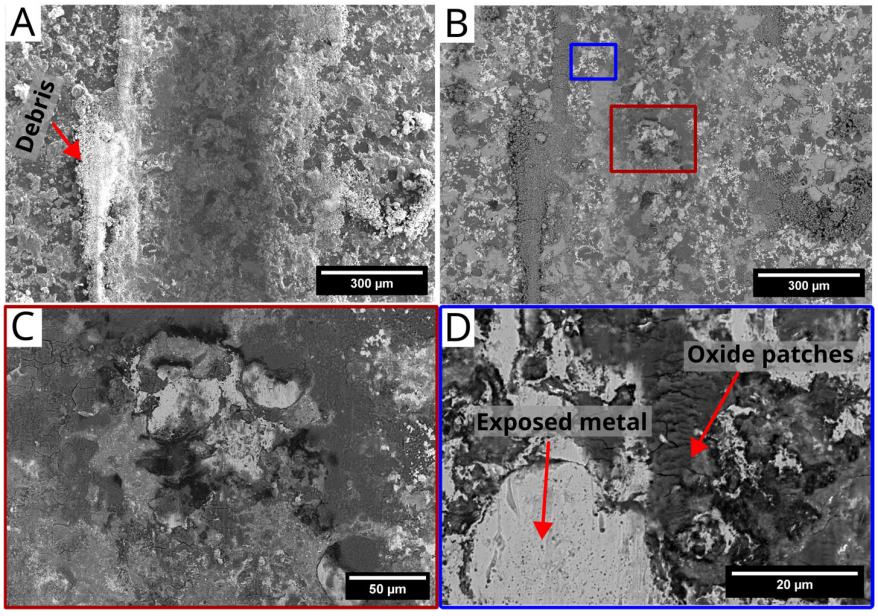

Figure 10. SEM images of the heat-treated coating after wear testing in room temperature conditions: (**A**) SE image of the track and (**B**) BSE image of the same location; (**C**,**D**) are higher magnification images of (**B**).

Raman was used on the wear tracks to determine the phases on the surface after the tests, and the results are shown in Figure 9E. From the sample tested at room temperature, barely any signal was detected on the wear tracks, suggesting that the components being formed at the contact interface are not Raman active. At higher temperatures, the only peak that can be observed inside the wear track can be correlated to NiO. However, unworn regions of the coating showed copper oxidation during the high-temperature testing (i.e., peaks of CuO at 296 cm^{-1}, 342 cm^{-1}, 630 cm^{-1} and 943 cm^{-1}) [25].

The wear track of the samples tested at room temperature and high-temperature conditions after heat treatment was also investigated. In Figure 10A,B a part of the wear track is observed. In it, accumulation of debris at the edges is indicated in Figure 10A. Inside the track, the oxide layer is partially removed, and some of the metallic splats are exposed (bright contrast in Figure 10C). Furthermore, some oxide patches start to be formed, as indicated in Figure 10D.

When testing at 300 °C, the heat-treated sample, a different behavior is observed, as shown in Figure 11. A more homogeneous layer is formed at the top surface, suggesting the plastic deformation, smearing, and mixing of some of the components. EDS analysis in the light gray region of Figure 11C has shown the presence of copper, nickel, and oxygen as main components, but also barium, cobalt, and aluminum, while the dark spots show the presence of aluminum, copper, and oxygen.

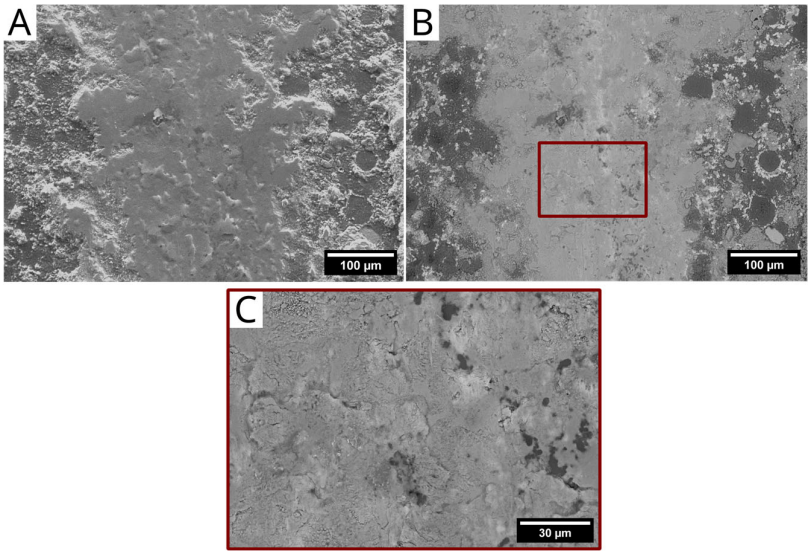

Figure 11. Top view of the wear track: (**A**) SE image showing smooth regions at the wear track, (**B**) BSE image, and (**C**) higher magnification BSE image on the middle of the wear track.

3.5. Counterface Characterization

SEM images of the counterfaces tested against the as-sprayed and heat-treated samples at room temperature and at 300 °C are shown in Figure 12, and the EDS analysis of the marked regions is shown in Table A2, Appendix A. For the as-sprayed samples, accumulation of debris was observed both after room temperature (Figure 12A) and elevated temperature (Figure 12B) conditions. At room temperature, material transfer from the coating to the counterface is observed, especially at the edges of the wear scar in the form of debris accumulation. Such a region has a high content of aluminum (25.3 ± 0.3 wt.%), nickel (23 ± 2 wt.%), oxygen (18 ± 2 wt.%), cobalt (13 ± 1 wt.%), chromium (10.8 ± 0.9 wt.%) and copper (6 ± 2 wt.%). The high content of aluminum indicates that either a signal from the counterface is being considered, or some of this debris is from the counterface. In the contact region, some spots of oxides being attached to the counterface are also observed.

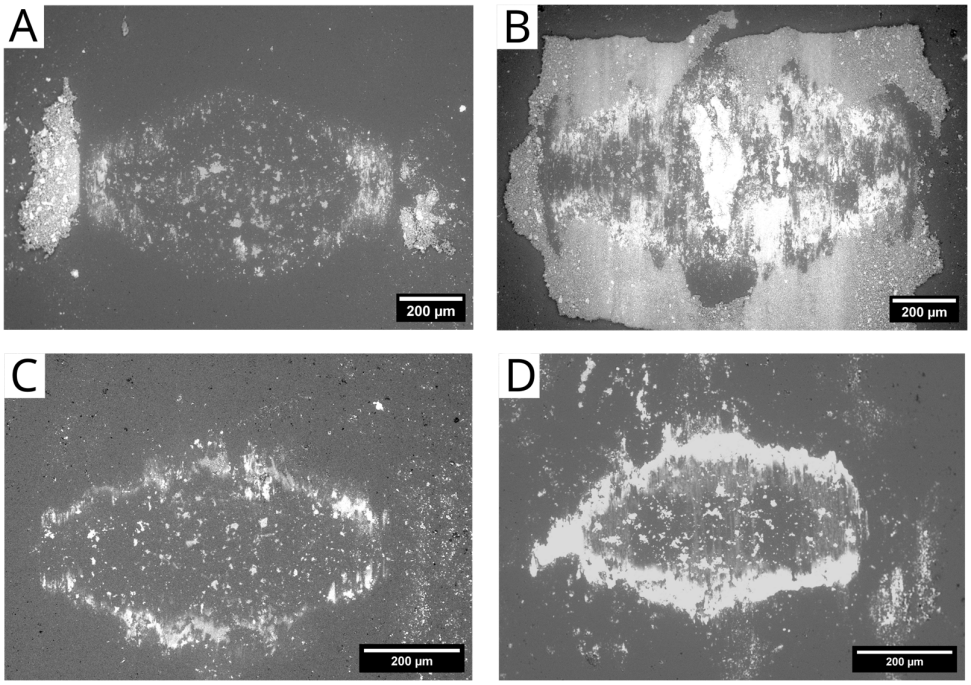

Figure 12. BSE images of alumina counterfaces tested against (**A**) as-sprayed coating tested in room temperature conditions; (**B**) as-sprayed coating at 300 °C; (**C**) heat-treated coating tested at room temperature; and (**D**) heat-treated coating at 300 °C.

At elevated temperature (Figure 12B for as-sprayed and Figure 12D for heat-treated condition), more accumulation of debris is observed on the counterface, at the edges of the contact region. Furthermore, material transfer seems to be more present in such conditions, with large areas of material being attached to the counterface in the contact region. Raman spectra were collected on all counterfaces (Figure 13), all showing peaks attributed to NiO [25]. For the sample tested at elevated temperature, there is a shift to the right, towards higher wavenumbers, which can be attributed to the convolution between the peaks of NiO and Cr_2O_3.

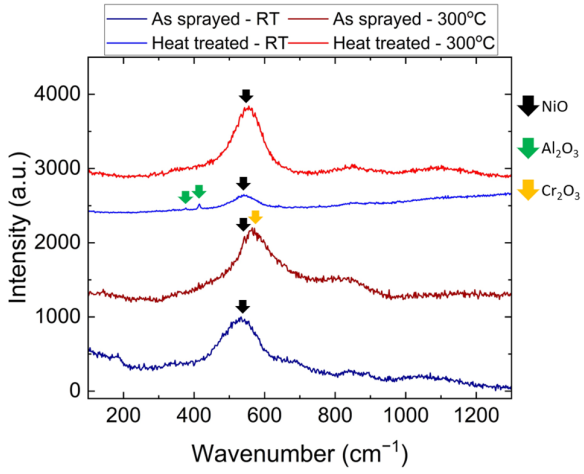

Figure 13. Raman spectra for all the counterfaces.

3.6. Wear Mechanisms

Under the tested condition, the as-sprayed coatings have shown similar wear performance when compared to other MCrAlY-based multicomponent coatings available in the literature [16]. Hao et al. found wear rates ranging from approximately 1×10^{-4} $mm^3/N{\cdot}m$

to approximately 3×10^{-4} mm^3/N·m when testing NiCoCrAlYTa-Ag-Mo coatings at temperatures of 25 at 400 °C, respectively [16], and approximately 1×10^{-4} mm^3/N·m when testing pure NiCoCrAlYTa at room temperature [23].

However, the present coating has shown worse performance when compared with coatings tested from previous studies of the authors [8,26], which analyzed the PS304 and PS400 coatings under the same sliding conditions, with the PS304 presenting wear rates in the order of 2–4 $\times 10^{-5}$ mm^3/N·m and the PS400 ranging from 2.6 $\times 10^{-6}$ mm^3/N·m to 2.02 $\times 10^{-4}$ mm^3/N·m depending on the tested temperatures.

Such poor performance is attributed mainly to the adhesive wear due to the presence of copper and the abrasive wear of the hard MCrAlY particles, causing elevated wear, elevated debris formation, and the unstable friction coefficient. It is proposed that material becomes attached to the counterface, and it is mechanically mixed and oxidized both at room temperature and at elevated temperature conditions. These islands of oxides are removed by the continuous reciprocating motion of the counterface and eventually leave the contact zone. Such activity continues throughout the whole test, which explains the high wear rate, the amount of debris being formed during the test and the fluctuations in the friction coefficient throughout the test. Such features are presented in Figure 14, which shows the different features being observed on the wear tracks of the different testing conditions.

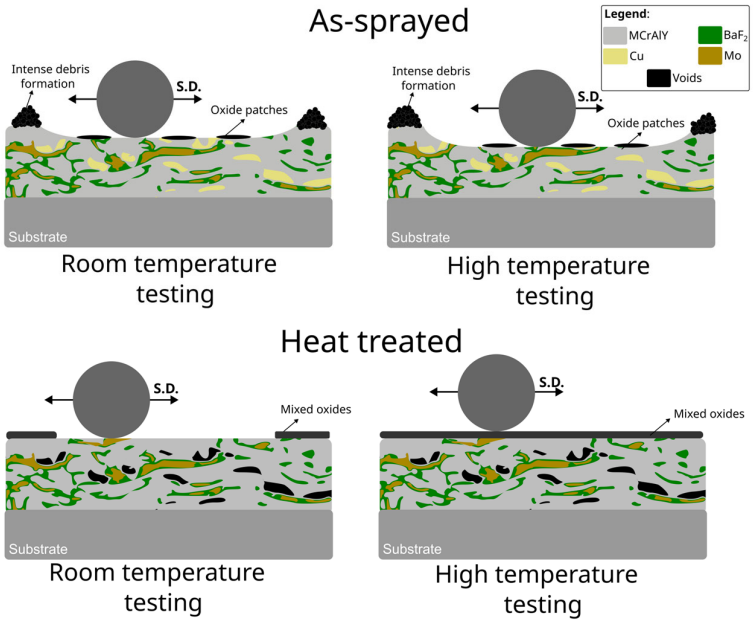

Figure 14. Drawing with the different features on the coating during tribological testing.

When the testing temperature is higher, the adhesion also increases, which explains the increased wear rates when testing in such temperatures. The fluctuation in the friction coefficient is still present, and so is the formation of debris. The wear track shows more polished patches, which indicates that these debris, now sintered and/or compacted, spend more time at the wear track, enough time to become sintered and acquire a more polished/smooth surface, which could contribute to the lower friction coefficient when compared to the room temperature testing. Then, those patches become detached and are removed from the contact zone, accumulating debris at the edges of the wear track.

After heat treating, the behavior of the coating is considerably different. Due to the formation of binary and ternary oxides at the surface, the contact changes from metal–oxide to oxide–oxide. Furthermore, the contact stresses are different when comparing as-sprayed and heat-treated samples, first due to the modification of the coating microstructure (such

as the change in the elastic modulus of the matrix component) and the oxidation of the top surface. Copper is no longer present as individual splats, but it is now part of the MCrAlY matrix, leaving voids in its original positions.

At room temperature, on the heat-treated coating, the wear of the sample happens by the partial removal of the top oxide layer, in some regions exposing the metallic splat underneath the oxide. Such removal occurs fast, in the initial stages of the test, and a tribolayer starts to be formed by a polishing effect on the contact region against alumina, with new patches of oxide material being formed in such a stage. At elevated temperatures, however, it is believed that the plastic deformation of the asperities and the spreading of the oxides at the surface are the only mechanisms in place. The formation of debris is minimal in such conditions, and some material transfer is observed to the counterface. The tribolayer, in such cases, shows the presence of all three types of oxides initially observed in the unworn surface of the heat-treated coating, namely, the aluminum oxide-rich phase, the copper/nickel oxide-rich phase, and the barium molybdate/chromate phase.

3.7. Oxidation and Hot Corrosion Behavior

Weight gain/loss were taken from the samples exposed to oxidation and hot corrosion conditions at temperatures ranging from 550 °C to 950 °C, as shown in Figure 15. For both conditions, the weight gain increased as testing temperature increased, driven by the incorporation of oxygen into the coating. However, the weight gain for the sample exposed to hot corrosion was always smaller than the one for oxidized samples. One possible explanation for such behavior is the vaporization of some volatile elements, most likely sulfur and/or oxygen from the salts.

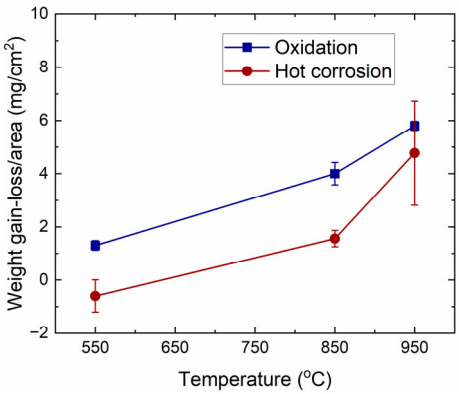

Figure 15. Comparison between oxidation and hot corrosion weight change.

Because of the low porosity of HVOF coatings, the salts did not penetrate through the coating, evaporating to the atmosphere inside the furnace, especially at 550 °C, in which a weight loss was observed instead of a weight gain. Considering that approximately 2 mg were spread on top of each coating and because of the way the weight gain/loss is calculated (final weight—initial weight with salt), it is possible that part of the components left the salt, giving a negative net weight.

The highest weight gain during hot corrosion (4.77 mg/cm^2) was observed at the test temperature of 950 °C, and it was considerably smaller than reported for silver-based plasma-sprayed coatings, such as the PS304 (21 mg/cm^2) and the PS400 (23.9 mg/cm^2) [11]. More importantly, different than it had been observed on the PS304 in previous studies [11], no spallation or delamination occurred, even though the same test procedure and conditions were used on these tests.

At lower temperatures, Xue-mei et al. determined the hot corrosion performance of NiCr coatings by testing them at 650 °C with K_2SO_4 and Na_2SO_4. The tests were performed

with and without an atmosphere of SO_3 in the furnace, and the authors measured weight gains in the order of 1–2 mg/cm^2 [27].

When compared to pure MCrAlY, the multicomponent coating also shows similar hot corrosion performance. Mohammadi et al. compared MCrAlY coatings produced by HVOF and low vacuum plasma spray and exposed the coatings to a mixture of Na_2SO_4 and $NaVO_3$ at 880 °C and measured a weight gain of approximately 2 mg/cm^2 after 24 h [28].

SEM images were taken on the cross-section of the coatings exposed to hot corrosion conditions, and they are shown in Figure 16A (850 °C) and Figure 16B (950 °C). The oxidized layer, in both conditions, is concentrated at the top surface. Furthermore, similar voids as the ones observed for heat-treated samples were observed, indicating that the diffusion of copper into the matrix occurs at lower temperatures than the heat-treating temperature.

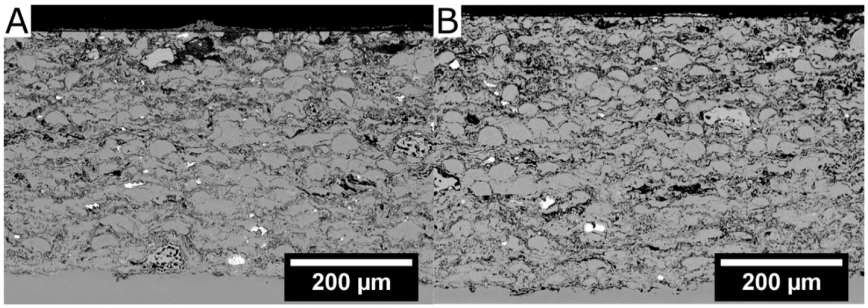

Figure 16. BSE images of the cross-section of the coatings after hot corrosion exposure at: (**A**) 850 °C and (**B**) 950 °C.

EDS images near the top surface at the cross-section of the sample hot corroded at 850 °C (Figure 17) show a thin layer of aluminum oxide covering the entire region and covering all the surfaces of the splats near the surface, which protects the exposed surface and the near-surface splat boundaries against oxidation and hot corrosion.

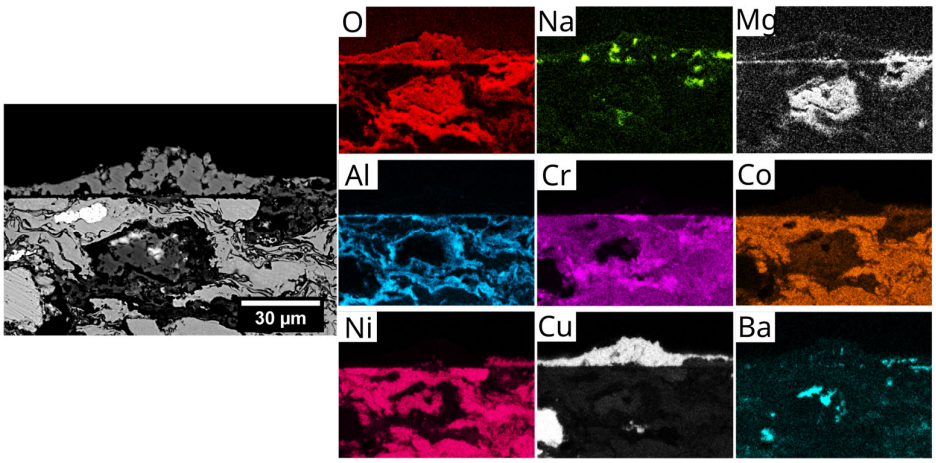

Figure 17. EDS mapping showing the presence of Mg and Na at the top surface after hot corrosion at 850 °C.

When analyzing the interface between coating and substrate (Figure 18), no presence of sulfur or any of the elements of the salts can be observed, indicating that the salt did not penetrate through the coating, and its influence was limited to the top surface of the coating. However, copper is observed to migrate also to the substrate and to the matrix element of the coating, which indicates that a stronger metallurgical bonding could be present. Such a hypothesis is further supported by the absence of coating spallation during the high-temperature tests, indicating strong adhesion of the coating to the substrate.

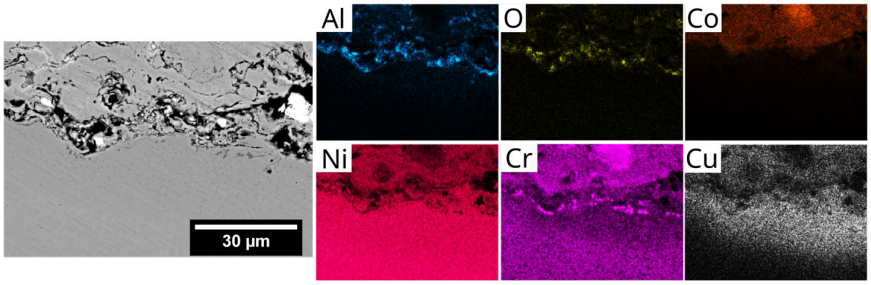

Figure 18. Image of the coating–substrate interface showing no sulfur or oxygen-based precipitates and demonstrating the diffusion of copper into the substrate.

4. Conclusions

In this study, an MCrAlY powder was sprayed with BaF_2, Cu, and Mo to produce a multicomponent coating with high-temperature capabilities and good tribological performance. It was expected that either copper or one of its oxides would act, at least to some extent, as a solid lubricant, helping to reduce friction and wear in testing temperatures between 25 and 300 °C. However, such an effect was not observed, and adhesive wear was present throughout the as-sprayed testing conditions, indicating that the adhesive component of the frictional force was the main reason for the high frictional values being observed. There was also an intense production of wear debris leaving the contact zone and accumulating into the edges of the track and into the counterface. Higher wear rates and higher friction coefficients were observed when compared to commonly used multicomponent coatings, such as the PS304 and the PS400.

To overcome the poor performance in the as-sprayed condition, the coating was heat treated to explore the possibility of forming beneficial binary and ternary oxides at the top surface, while enough time was provided to allow the interdiffusion of elements between the components. The results have shown a significant improvement in the performance of the coating, both at room and elevated temperature. Wear at room temperature happened by the partial removal of the oxide layer and the formation of a new mixed layer on top of the coating, allowing for reasonably low friction and low wear rates. On the other hand, when the coatings were tested at 300 °C, the oxides at the surface formed a smooth tribolayer covering the whole track, and a friction value of approximately 0.38 was observed.

Such modification on the coating microstructure and the improvement on the tribological performance prove the feasibility of forming beneficial oxides with this coating mixture by heat treating. Although the heat treatment lasted for only four hours, the high temperature induced the modification of several of the components and allowed the interdiffusion between the elements, and in some locations at the surface, even partial melting of some of the components.

When exposed to oxidation and hot corrosion conditions, these coatings have shown minor weight gain in most conditions due to the performance of the MCrAlY matrix combined with the low porosity resulting from the HVOF process, thus outperforming currently used plasma-sprayed multicomponent coatings and protecting the substrate against the harmful effects of oxidation and molten salts.

Author Contributions: Conceptualization, B.C.N.M.d.C., N.S., M.M, P.S., C.M. and R.R.C.; methodology, B.C.N.M.d.C., N.S., P.S., C.M. and R.R.C.; investigation, B.C.N.M.d.C. and N.S.; resources, M.M, C.M. and R.R.C.; writing—original draft preparation, B.C.N.M.d.C.; writing—review and editing, R.R.C.; visualization, B.C.N.M.d.C.; supervision, C.M. and R.R.C.; project administration, M.M., C.M. and R.R.C.; funding acquisition, M.M, P.S., C.M. and R.R.C. All authors have read and agreed to the published version of the manuscript.

Funding: This research was funded by the Natural Sciences and Engineering Research Council (NSERC) (project number CRDPJ 530409-18) and the Consortium for Research and Innovation in Aerospace in Quebec (CRIAQ) (project number MANU-1719). Dr. BCNMC would also like to thank the McGill Engineering Doctoral Award (MEDA) granted in his name.

Data Availability Statement: The raw data supporting the conclusions of this article will be made available by the authors upon request.

Acknowledgments: The authors would like to acknowledge the support of Fadhel Ben Ettouil with the coating deposition. The authors would also like to acknowledge Eutectic Canada for providing Mo and BaF_2 powders for the project.

Conflicts of Interest: Author Mary Makowiec was employed by the company Pratt & Whitney. The remaining authors declare that the research was conducted in the absence of any commercial or financial relationships that could be construed as a potential conflict of interest.

Appendix A

Table A1. EDS point analysis on the wear track in wt.%.

Elements	1	2	3	4	5
Ni	42 ± 1	25.0 ± 0.2	30 ± 2	31 ± 1	13 ± 4
Co	21.4 ± 0.6	12.7 ± 0.2	16 ± 1	17 ± 1	8 ± 2
Cr	20.0 ± 0.9	11.1 ± 0.4	14 ± 1	15 ± 1	6 ± 1
Al	8.6 ± 0.7	5.2 ± 0.6	5.5 ± 0.3	5 ± 1	2 ± 1
Y	0.4 ± 0.5	0	0	0	0
Ta	4.6 ± 0.2	2.6 ± 0.2	3.0 ± 0.2	3.2 ± 0.3	1.0 ± 0.9
O	1.4 ± 0.4	26 ± 2	19 ± 3	4.5 ± 0.1	13 ± 1
Ba	0	1.9 ± 0.2	2.2 ± 0.3	0.4 ± 0.4	1.7 ± 0.7
F	0	1.0 ± 0.7	1.1 ± 0.8	0	1.2 ± 0.3
Mo	0	1.8 ± 0.8	0.6 ± 0.4	0	0
Cu	2.7 ± 0.9	15 ± 3	9 ± 1	23 ± 5	53 ± 11

Table A2. EDS point analysis on the counterface in wt.%.

Elements	1	2	3	4	5	6
Ni	23 ± 2	2.5 ± 0.5	11.8 ± 0.1	22.0 ± 0.8	24.7 ± 0.5	21.6 ± 0.3
Co	13 ± 1	1.4 ± 0.3	6.6 ± 0.3	11.7 ± 0.5	13.1 ± 0.1	12.0 ± 0.2
Cr	10.9 ± 0.9	1.1 ± 0.2	5.7 ± 0.2	10.0 ± 0.3	11.0 ± 0.5	9.5 ± 0.2
Al	25.3 ± 0.3	52.6 ± 0.7	33.6 ± 0.3	23 ± 1	18.7 ± 0.5	18.1 ± 0.2
Y	0	0	0	0	0	0
Ta	1.8 ± 0.3	0.8 ± 0.1	1.7 ± 0.1	2.3 ± 0.2	3.2 ± 0.1	2.9 ± 0.1
O	18 ± 2	42 ± 2	36.0 ± 0.4	22.9 ± 0.9	19 ± 1	25.8 ± 0.4
Ba	1.5 ± 0.1	0	1.0 ± 0.2	1.6 ± 0.2	1.8 ± 0.1	1.7 ± 0.1
F	0	0	0	0	0.6 ± 0.9	0
Mo	0.8 ± 0.7	0	0	0	0.7 ± 0.1	0.9 ± 0.1
Cu	6 ± 2	0	3.6 ± 0.6	6 ± 1	7.0 ± 0.3	7.4 ± 0.1

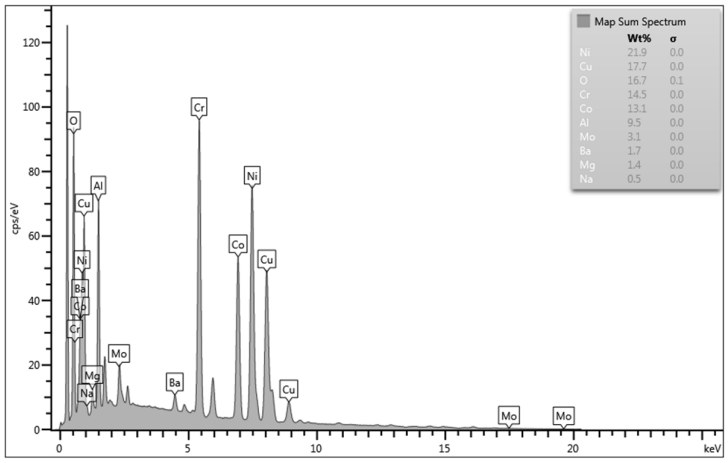

Figure A1. Sum spectrum of the mapping on Figure 16.

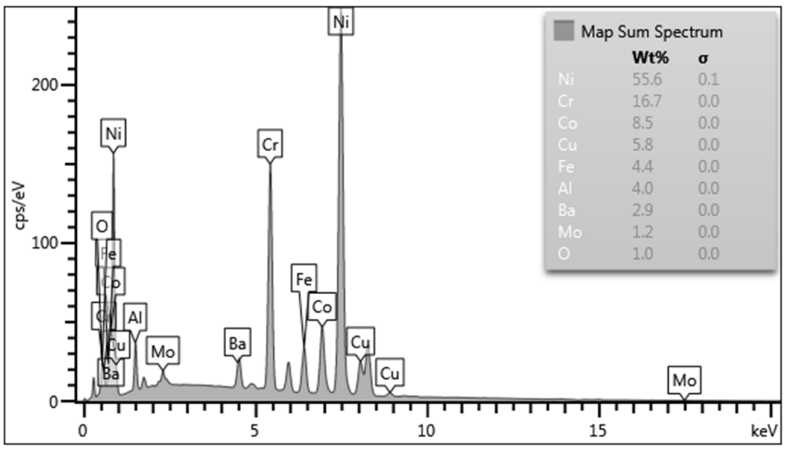

Figure A2. Sum spectrum of the mapping on Figure 17.

References

1. Sliney, H.E. Wide temperature spectrum self-lubricating coatings prepared by plasma spray. *Thin Solid Film.* **1979**, *64*, 211–217. [CrossRef]
2. Dellacorte, C.; Fellenstein, J.A. The effect of compositional tailoring on the thermal expansion and tribological properties of PS300: A solid lubricant composite coating. *Tribol. Trans.* **1997**, *40*, 639–642. [CrossRef]
3. Balic, E.E.; Blanchet, T.A. Thrust-washer tribological evaluation of PS304 coatings against Rene 41. *Wear* **2005**, *259*, 876. [CrossRef]
4. Blanchet, T.A.; Kim, J.-H.; Calabrese, S.J.; Dellacorte, C. Thrust-washer evaluation of self-lubricating PS304 composite coatings in high temperature sliding contact. *Tribol. Trans.* **2002**, *45*, 491–498. [CrossRef]
5. DellaCorte, C.; Zaldana, A.R.; Radil, K.C. A systems approach to the solid lubrication of foil air bearings for oil-free turbomachinery. *Trans. ASME* **2004**, *126*, 200–207. [CrossRef]
6. Wang, W. Application of a high temperature self-lubricating composite coating on steam turbine components. *Surf. Coat. Tech.* **2004**, *177–178*, 12–17. [CrossRef]
7. Stanford, M.K.; Yanke, A.M.; DellaCorte, C. *Thermal Effects on a Low Cr Modification of PS304 Solid Lubricant Coating*; NASA: Hanover, MD, USA, 2004.
8. de Castilho, B.C.N.M.; Sharifi, N.; Alidokht, S.; Harrington, K.; Stoyanov, P.; Moreau, C.; Chromik, R. Short-time exposure oxidation studies on multi-component coatings and their influence on tribological behavior. *Wear* **2021**, *477*, 203892. [CrossRef]
9. DellaCorte, C.; Edmonds, B.J. *NASA PS400: A New High Temperature Solid Lubricant Coating for High Temperature Wear Applications*; NASA Center for Aerospace Information: Hanover, MD, USA, 2009.
10. Radil, K.; DellaCorte, C. The performance of PS400 subjected to sliding contact at temperatures from 260 to 927 °C. *Tribol. Trans.* **2017**, *60*, 957–964. [CrossRef]
11. de Castilho, B.C.N.M.; Sharifi, N.; Makowiec, M.E.; Stoyanov, P.; Moreau, C.; Chromik, R.R. Oxidation and hot corrosion behavior of multicomponent coatings produced by atmospheric plasma spray. *J. Mater. Sci.* **2024**, *59*, 10508–10525. [CrossRef]

12. Kim, J.-H.; Blanchet, T.A.; Calabrese, S.J. High velocity oxyfuel deposition for low surface roughness PS304 self-lubricating composite coatings. *Tribol. Trans.* **2004**, *47*, 157–169. [CrossRef]
13. Shi, X.; Xu, Z.; Wang, M.; Zhai, W.; Yao, J.; Song, S.; Din, A.Q.U.; Zhang, Q. Tribological behavior of TiAl matrix self-lubricating composites containing silver from 25 to 800 °C. *Wear* **2013**, *303*, 486–494. [CrossRef]
14. Jeng, M.-C.; Soong, Y.-L. Wear behaviour of solid lubricants Ag and BaF_2-CaF_2 obtained by laser surface cladding. *Surf. Coat. Tech.* **1993**, *57*, 145–150. [CrossRef]
15. Chen, J.; An, Y.; Yang, J.; Zhao, X.; Yan, F.; Zhou, H.; Chen, J. Tribological properties of adaptive NiCrAlY-Ag-Mo coatings prepared by atmospheric plasma spraying. *Surf. Coat. Tech.* **2013**, *235*, 521–528. [CrossRef]
16. Hao, E.; An, Y.; Chen, J.; Zhao, X.; Hou, G.; Chen, J.; Gao, M.; Yan, F. In-situ formation of layer-like Ag_2MoO_4 induced by high-temperature oxidation and its effect on the self-lubricating properties of NiCoCrAlYTa/Ag/Mo coatings. *J. Mat. Sci. Technol.* **2021**, *75*, 164–173. [CrossRef]
17. Li, B.; Gao, Y.; Jia, J.; Han, M.; Guo, H.; Wang, W. Influence of heat treatments on the microstructure as well as mechanical and tribological properties of NiCrAlY-Mo-Ag coatings. *J. Alloys Compd.* **2016**, *686*, 503–510. [CrossRef]
18. Torres, H.; Ripoll, M.R.; Prakash, B. Tribological behaviour of self-lubricating materials at high temperatures. *Int. Mat. Rev.* **2018**, *63*, 309–340. [CrossRef]
19. Yuan, J.; Zhu, Y.; Ji, H.; Zheng, X.; Ruan, Q.; Niu, Y.; Liu, Z.; Zeng, Y. Microstructures and tribological properties of plasma sprayed WC-Co-Cu-BaF_2/CaF_2 self-lubricating wear resistant coatings. *Appl. Surf. Sci.* **2010**, *256*, 4938–4944. [CrossRef]
20. Gao, H.; Otero-de-la-Roza, A.; Gu, J.; Stones, D.; Aouadi, S.M.; Johnson, E.R.; Martini, A. (Ag,Cu)-Ta-O ternaries as high-temperature solid-lubricant coatings. *ACS Appl. Mater. Interfaces* **2015**, *7*, 15422–15429. [CrossRef]
21. Oliver, W.C.; Pharr, G.M. An improved technique for determining hardness and elastic modulus using load and displacement sensing indentation experiments. *J. Mater. Res.* **1992**, *7*, 1564–1583. [CrossRef]
22. Hao, E.; Zhao, X.; An, Y.; Deng, W.; Zhou, H.; Chen, J. The effect of pre-oxidation on microstructure, mechanical properties and high-temperature tribological behaviors of HVOF-sprayed NiCoCrAlYTa coating. *Appl. Surf. Sci.* **2019**, *489*, 187–197. [CrossRef]
23. Hao, E.; An, Y.; Zhao, X.; Zhou, H.; Chen, J. NiCoCrAlYTa coatings on nickel-base superalloy substrate: Deposition by high velocity oxy-fuel spraying as well as investigation of mechanical properties and wear resistance in relation to heat-treatment duration. *Appl. Surf. Sci.* **2018**, *462*, 194–206. [CrossRef]
24. Han, Y.; Chen, H.; Gao, D.; Yang, G.; Liu, B.; Chu, Y.; Fan, J.; Gao, Y. Microstructural Evolution of NiCoCrAlHfYSi and NiCoCrAlTaY Coatings Deposited by AC-HVAF and APS. *J. Therm. Spray. Technol.* **2017**, *26*, 1758–1775. [CrossRef]
25. RRUFF Project: Database of Raman Spectra, X-Ray Diffraction and Chemistry Data. Available online: https://rruff.info/ (accessed on 15 June 2024).
26. de Castilho, B.C.N.M.; Munagala, V.N.V.; Alidokht, S.A.; Sharifi, N.; Bessette, S.; Makowiec, M.E.; Gauvin, R.; Stoyanov, P.; Moreau, C.; Chromik, R.R. Insights on Silver Migration Mechanisms and their Influence on the Wear Behavior of Thermally Sprayed Self-lubricating Coatings Up to 350 °C. *Tribol. Lett.* **2022**, *70*, 120. [CrossRef]
27. Xue-mei, O.; Zhi, S.; Min, S.; Duan-lian, Z. Hot-corrosion mechanism of Ni-Cr coatings at 650 °C under different simulated corrosion conditions. *J. China Univ. Min. Technol.* **2008**, *18*, 444–448.
28. Mohammadi, M.; Javadpour, S.; Jahromi, S.A.J.; Kobayashi, A. Characterization and hot corrosion performance of LVPS and HVOF-CoNiCrAlYSi coatings. *Vacuum* **2012**, *86*, 1458–1464. [CrossRef]